
INVERSE SET ESTIMATION AND INVERSION OF SIMULTANEOUS CONFIDENCE INTERVALS

Junting Ren

Division of Biostatistics
University of California San Diego
j5ren@ucsd.edu

Fabian J.E. Telschow

Institute of Mathematics
Humboldt Universität zu Berlin
fabian.telschow@hu-berlin.de

Armin Schwartzman

Division of Biostatistics and Halıcıoğlu Data Science Institute
University of California San Diego
armins@ucsd.edu

ABSTRACT

The preimage or inverse image of a predefined subset of the range of a deterministic function, called inverse set for short, is the set in the domain whose image equals that predefined subset. To quantify the uncertainty in the estimation of such a set, we propose data-dependent inner and outer confidence sets that are sub- and super-sets of the true inverse set with a given confidence. Existing methods require strict assumptions, and the predefined subset of the range is usually an excursion set for only one single level. We show that by inverting pre-constructed simultaneous confidence intervals, commonly available for different kinds of data, multiple confidence sets of multiple levels can be simultaneously constructed with the desired confidence non-asymptotically. The method is illustrated on dense functional data to determine regions with rising temperatures in North America and on logistic regression data to assess the effect of statin and COVID-19 on clinical outcomes of in-patients.

Keywords Inverse set · Simultaneous confidence band

1 Introduction

The preimage or inverse image of a set $U \subset \mathbb{R}$ under a deterministic function $\mu : \mathcal{S} \mapsto \mathbb{R}$, called *inverse set* for short here, is defined as $\mu^{-1}(U) = \{s \in \mathcal{S} : \mu(s) \in U\}$: the set in the closed domain \mathcal{S} such that the function output $\mu(s)$ is in a predefined subset U of the range in \mathbb{R} . For example, if $U = [c, +\infty)$, then $\mu^{-1}(U)$ is the excursion set of μ above the level c . Suppose μ is unknown but data is available to construct an estimator $\hat{\mu}$. A point estimate of the inverse set is $\hat{\mu}^{-1}(U)$. We wish to quantify the uncertainty in the estimation of such an inverse set. We do so by constructing data-dependent inner and outer confidence set $\text{CS}_{\text{in}}(U)$ and $\text{CS}_{\text{out}}(U)$ that are sub- and super-sets of this inverse set:

$$\text{CS}_{\text{in}}(U) \subseteq \mu^{-1}(U) \subseteq \text{CS}_{\text{out}}(U). \quad (1.1)$$

This is analogous to confidence intervals, with the “lower bound” being $\text{CS}_{\text{in}}(U)$ and the “upper bound” being $\text{CS}_{\text{out}}(U)$. The setting we present here is applicable to many statistical problems. For example, μ could be a mean function or a density function. The closed domain \mathcal{S} could be an uncountable subset of \mathbb{R}^D such as the domain of functional data or the sample space of continuous predictors in a regression problem, or a finite discrete set $\{1, 2, 3, \dots, K\}$ such as indexes of regression coefficients.

1.1 Motivation

Studies are often interested in finding excursion sets of the form $\{s \in \mathcal{S} : \mu(s) > 0\}$. Hypothesis testing and p-values are widely utilized to locate these sets. For example in medical imaging, voxel-wise [1] or cluster-wise [2] hypothesis

testing is used to discover activation regions of the brain in fMRI scans. In genome-wide association studies, thousands of features in a genome-wide data set are tested against some null hypothesis to find genetic loci associated with physical characteristics or diseases [3, 4]. More traditionally in regression models, when the number of predictors is small, analysis of variance (ANOVA) is performed to test whether multiple coefficients are significantly different from 0 [5]. In the above examples, finding an excursion set such as $\{s \in \mathcal{S} : \mu(s) > 0\}$ is equivalent to finding the inverse set $\mu^{-1}(U)$ where $U = (0, +\infty)$.

In the above situations, hypothesis testing is used as a tool for finding where the signal is. There are two main reasons why we favor estimating the inverse set $\mu^{-1}(U)$ over performing hypothesis testing. First, with big data and large sample sizes, even a small difference that is not practically significant will yield a significant p-value [6, 7, 8, 9]. Inference on non-zero effect sizes is more informative. An effect larger than or equal to some meaningful constant c corresponds to $U = [c, +\infty)$. Second, hypothesis testing does not provide inference on localization formally or the uncertainty of localization. For example, in a global ANOVA test in multiple regression, the p-value only conveys that at least one coefficient is different from 0 but not which specific coefficient parameter is. Similarly for medical imaging, the cluster-level p-value only states that significant activation is somewhere inside the region, but not where inside the region it is [10].

1.2 Existing inverse set estimation methodology and pitfalls

Inverse set estimation methods are applied in different fields, such as astronomy [11], medical imaging [12, 13, 9], dose-effect finding [14], and geoscience [15]. Furthermore, there is a growing trend to quantify the effect size for genomic regions rather than just testing the null hypothesis [16, 17], where inverse set estimation methods can be utilized to quantify the uncertainty of genomic regions with effects greater than a certain threshold.

However, most existing inverse set estimation methods are only applicable to specific kinds of data and require strict assumptions. For example, the method from [18] is proposed for dense functional data, which requires the underlying true mean function to be continuous, and the coverage probability is only asymptotic for large sample size. Other methods are specifically designed for scenarios where the function μ is a density function [19, 20, 21]. The method proposed by [14] only works for logistic regression and provides no theoretical guarantee on the coverage rate. Inverse set methods have been also developed for stochastic processes (random functions), but they require the process itself to be Gaussian and data must be observed on a fixed grid [22, 23, 24].

The additional significant issue with all the inverse set estimation methods above is that the estimated confidence sets are only valid for a single level c , for example, estimating the set $\mu^{-1}[c, +\infty)$ for a fixed level c . Like in hypothesis testing, for the inference to be valid, the level c needs to be pre-specified. However, there is no general consensus on which level c to use and the meaningful levels differ from problem to problem. In most practical situations, it is unreasonable to expect the level c would be known beforehand without investigating the data. Furthermore, researchers might be interested in estimating inverse sets for multiple levels. Therefore, it is crucial to develop inverse set estimation methods that will be valid for any level and maintains the overall type I error rate.

1.3 Simultaneous inverse set estimation

The main idea of this paper is that simultaneous confidence intervals (SCIs) or simultaneous confidence bands (SCBs) can be used to construct confidence sets for estimating the inverse sets of multiple levels c while controlling the error rate. Originally, SCIs and SCBs are constructed to quantify the uncertainty of the data's estimated mean functions indexed by a discrete or continuous domain. Inference and statistical tests can be made for the true mean function on the entire domain. For example, a typical question for regression coefficients or for functional data is whether the true mean function on the indexing domain is greater than $c = 0$. The key observation is that SCIs and SCBs can be interpreted and modified to construct confidence sets simply by inversion.

As an illustration, Figure 1 shows a toy example of dense functional data where we are interested in estimating the sets where the mean function μ is greater than certain levels. One of the inverse sets we are trying to estimate is $\mu^{-1}[0.2, +\infty)$, represented by the union of the green and red horizontal lines on top of the dashed horizontal line at 0.2. The point estimate of this inverse set is $\hat{\mu}^{-1}[c, +\infty)$ (not shown for simplicity). The inner and outer sets we propose are the inverse sets of the lower and upper SCBs. It is intuitive to classify the region with the 95% SCB's lower band above level $c = 0.2$ as $CS_{in}[c, +\infty)$ (colored by the red horizontal line), where we estimate that $\forall s \in CS_{in}[c, +\infty), \mu(s) \geq c$. This is often used as an ad-hoc way of finding regions with significant signals, for example in [25, 26]. The statement $CS_{in}[c, +\infty) \subseteq \mu^{-1}[c, +\infty)$ should be correct with at least 95% probability, and this is indeed proven in our proposition 1. However, it turns out this is quite conservative. The detailed properties have not been formally studied in the literature.

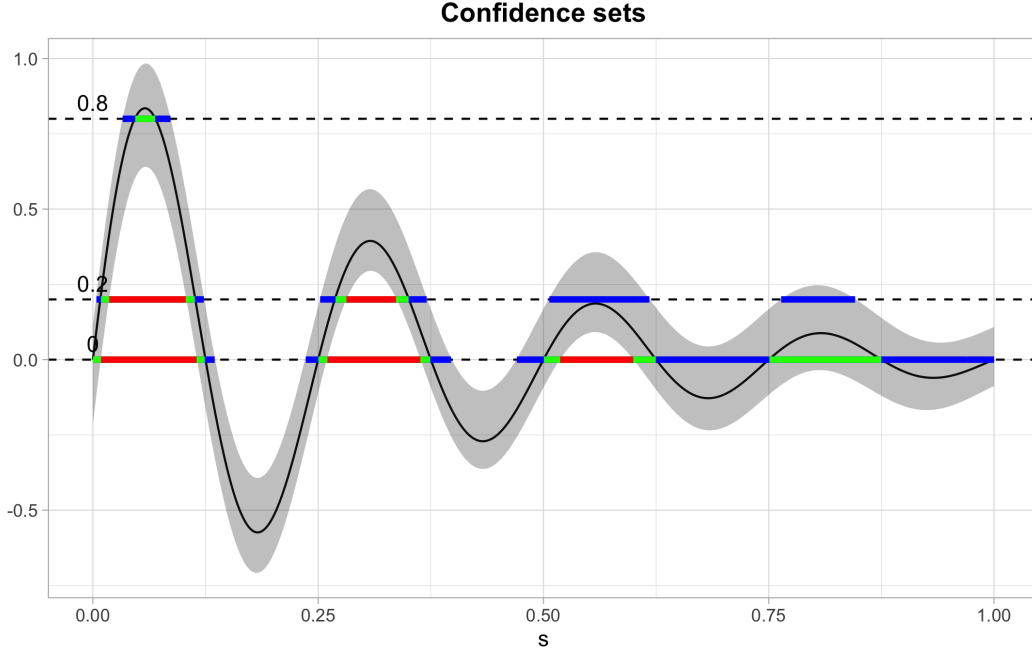


Figure 1: 1D dense functional data simulation showcase. Demonstration of using SCB to find regions of s where the true mean is greater than or equal to the three levels 0, 0.2, 0.8 for 1D dense functional data. The gray shaded area is the 95% SCB, the solid black line is the true mean. The red horizontal line shows the inner confidence sets (where the lower SCB is greater than the corresponding level) that are contained in the true inverse set represented by the union of the green and red horizontal line (where the true mean is greater than the corresponding levels); the outer confidence sets are the union of the blue, green and red line (where the upper SCB is greater than the corresponding levels) and contain both the true inverse sets and the inner confidence sets.

Building on this idea, we construct confidence sets, that are valid for all levels $c \in \mathbb{R}$ simultaneously, by simply inverting pre-built SCIs for discrete domains or SCBs for continuous domains. The only assumption we require is that the SCIs or SCBs are valid with a predetermined type I error rate. This guarantees that the coverage probability of our confidence sets for all $c \in \mathbb{R}$ is exactly the same as the SCI or SCB coverage rate. In real data applications and even simulation studies, SCBs are constructed on a grid of discrete points that are essentially “dense” SCIs. Therefore, for brevity, we unify the two terms and refer to them both as SCIs.

Here are the two additional appealing properties of our inverse set estimation method:

- It can be applied to any domain as long as there is a method for constructing SCI. This includes regression, 1D or 2D functional data, etc. After constructing SCIs with simultaneous $\alpha\%$ type I error rate, confidence sets of any number of levels can be constructed with correct inclusions with at least $1 - \alpha$ probability.
- Inverse confidence sets provide meaningful visualization of SCIs with a spatial interpretation. For example, SCIs are usually hard to visualize for two-dimensional data. Using contours of the confidence sets, we can draw “probability contour maps” as demonstrated in Figure 2 and 3. Unlike informal contour maps for 2D data, our “probability contour lines” convey formal spatial region uncertainty statements. We display two ways of visualizing multiple confidence sets for multiple levels. The visualization in the first row of Figure 2 and 3 is helpful when the researcher is interested in finding the inner or outer confidence sets for multiple levels simultaneously. The researcher may want to view the second row if the goal is to focus on finding the excursion set for a specific level.

Inspired by Goeman [27, 28], our inverse set estimation method guards against “data peeking” in exploratory data analysis, allowing the researcher to build confidence sets for any level c without worrying about losing control of type I error rate. When constructing confidence sets for a fixed number of levels, we investigate the conservativeness of the coverage rate compared to the SCIs. We find that under certain setups, the coverage rates are close to the SCI coverage rate.

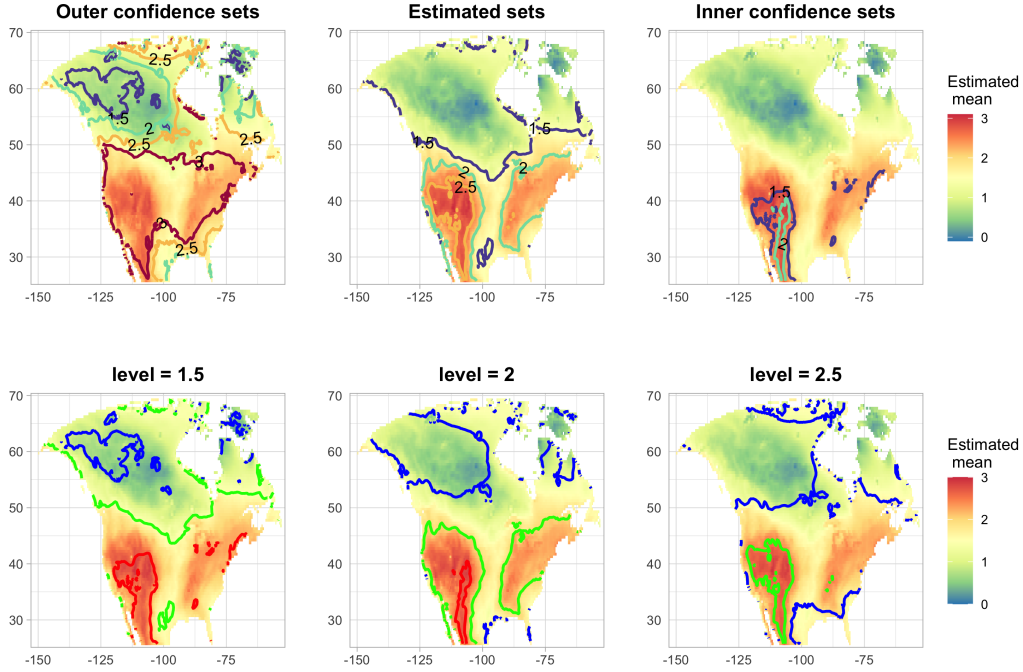


Figure 2: Confidence sets for the increase of the mean summer temperature (June–August) in North America between the 20th and 21st centuries according to the specific climate model analyzed in [18]. Heat maps show the estimate of the mean difference. The first row displays the contours of the outer confidence sets, estimated inverse set, and the inner confidence sets, for various levels. The three plots in the second row display the confidence sets for the inverse sets, where the estimated mean difference is greater or equal to the individual level 1.5, 2.0, or 2.5 respectively. In the second row, the blue line is the contour of the outer confidence set, the green line is the contour of the estimated inverse set and the red line is the contour of the inner confidence set.

1.4 Existing simultaneous confidence interval methods

Since the proposed inverse confidence sets estimation method is based on SCIs, it is worth reviewing existing SCI methods, to which our method would be applicable. For dense functional data, researchers constructed SCIs based on functional central limit theorems in the Banach space using Monte-Carlo simulations with an estimate of the limiting covariance structure [29, 30, 31], based on bootstrap [32, 33], and based on the Gaussian Kinematic formula [34]. For sparse functional data, SCIs are built using functional principal component analysis [35, 36]. For high dimensional data such as genomics data with discrete indexing, valid SCIs are built for high dimensional but a finite number of parameters before selection [37] or after selection [38, 39]. For survival data, SCIs for survival functions are built using Greenwood’s variance formula under large sample sizes [40], as well as SCIs for the difference or ratio of two survival functions [41, 42]. For regression problems, researchers are often interested in how the response y changes with a vector of predictors x , or the magnitude of the regression coefficients. Therefore, SCIs can be constructed for y on the range of x [43, 44, 45], or for multiple regression coefficients [46, 47].

1.5 Outline

After stating and proving the main theorem and corollaries in Section 2, we present the results of simulation studies that validate our method for continuous domains using dense functional data and regression mean prediction on a fine grid of predictors. For discrete domains, confidence sets for regression coefficients are constructed using simulated datasets, and the results are shown in Section 3. In addition, for different correlation structures between the estimated means $\hat{\mu}(s)$ in the domain \mathcal{S} , we demonstrate how conservative the method is when only a finite number of confidence sets are constructed, compared to the SCI nominal coverage rate. We showcase the advantages of our model over [18] in both the simulations and the real data application. Following the simulations, we exhibit motivating applications in two different kinds of data: probability contour for mean temperature difference map, and logistic regression for

determining whether statin is protective against the severe outcome of Coronavirus disease 2019 (COVID) patients in Section 4. We conclude with a brief discussion in Section 5.

2 Theory

2.1 Setup

The goal of inverse set estimation is to estimate the set $\mu^{-1}(U) = \{\mathbf{s} \in \mathcal{S} : \mu(\mathbf{s}) \in U\}$ where $\mu : \mathcal{S} \mapsto \mathbb{R}$ is an unknown deterministic function, U is a fixed subset of \mathbb{R} , and \mathcal{S} is a closed indexing set. The "point estimator" of the true inverse set is:

$$\hat{\mu}^{-1}(U) = \{\mathbf{s} \in \mathcal{S} : \hat{\mu}(\mathbf{s}) \in U\}.$$

Similar to the point estimate of a scalar parameter, we need a "lower bound" and an "upper bound" for the estimated inverse set. Therefore, we introduce the data-dependent outer confidence set $\text{CS}_{\text{out}}(U)$ and the data-dependent inner confidence set $\text{CS}_{\text{in}}(U)$ with the goal that the true inverse set $\mu^{-1}(U) = \{\mathbf{s} \in \mathcal{S} : \mu(\mathbf{s}) \in U\}$ is "sandwiched" within them:

$$\text{CS}_{\text{in}}(U) \subseteq \mu^{-1}(U) \subseteq \text{CS}_{\text{out}}(U).$$

2.2 Estimating inverse upper excursion sets

The central idea of this article is that such confidence sets can be obtained by inverting SCIs. Let $\hat{B}_l(\mathbf{s})$ and $\hat{B}_u(\mathbf{s})$ denote the estimated lower and upper SCI functions at pre-specified level α such that:

$$\mathbb{P} \left[\forall \mathbf{s} \in \mathcal{S} : \hat{B}_l(\mathbf{s}) \leq \mu(\mathbf{s}) \leq \hat{B}_u(\mathbf{s}) \right] = 1 - \alpha$$

Because the function μ and the SCIs are generally not one-to-one functions, the inversion can get complicated depending on the interval U . We simplify this issue by setting U as half of the real line, and this is often the set that researchers are interested in. We can define the following *inverse upper excursion set* at level c as:

$$\mu^{-1}[c, +\infty) = \{\mathbf{s} \in \mathcal{S} : \mu(\mathbf{s}) \geq c\}$$

In addition, we define the following sets as the inner and outer confidence sets for the inverse upper excursion set $\mu^{-1}[c, +\infty)$ for a single level c :

$$\text{CS}_{\text{in}}[c, +\infty) := \hat{B}_l^{-1}[c, +\infty) = \left\{ \mathbf{s} \in \mathcal{S} : \hat{B}_l(\mathbf{s}) \geq c \right\}$$

$$\text{CS}_{\text{out}}[c, +\infty) := \hat{B}_u^{-1}[c, +\infty) = \left\{ \mathbf{s} \in \mathcal{S} : \hat{B}_u(\mathbf{s}) \geq c \right\}$$

In Figure 1, the red horizontal lines are the $\text{CS}_{\text{in}}[c, +\infty)$, whereas the union of red, green and blue horizontal lines are the $\text{CS}_{\text{out}}[c, +\infty)$. Henceforth, we distinguish between the inference when c is a single level and when the inference is simultaneous over multiple choices of the level c .

2.2.1 Single level confidence set from SCI

In [25, 26], after constructing a bootstrap percentile SCI, the authors claim that the true mean is greater than $c = 0$ in the region where the estimated lower interval is greater than 0. However, no probability or confidence statement is given. This is one of the ad-hoc examples of using SCI for inverse set estimation in applications. The following Proposition 1 provides a formal justification for the procedure above, stating that for a single level c , $\hat{B}_l^{-1}[c, +\infty)$ is a set such that we are at least 95% confident that $\forall \mathbf{s} \in \hat{B}_l^{-1}[c, +\infty), \mu(\mathbf{s}) \geq c$.

Proposition 1. *For a fixed level $c \in \mathbb{R}$, and SCIs with α type I family-wiser error rate, we have*

$$\mathbb{P} \left(\hat{B}_l^{-1}[c, +\infty) \subseteq \mu^{-1}[c, +\infty) \right) \geq \mathbb{P} \left(\forall \mathbf{s} \in \mathcal{S} : \hat{B}_l(\mathbf{s}) \leq \mu(\mathbf{s}) \leq \hat{B}_u(\mathbf{s}) \right) = 1 - \alpha$$

Proof. Define the following events

$$E := \left\{ \hat{B}_l^{-1}[c, +\infty) \subseteq \mu^{-1}[c, +\infty) \right\},$$

and

$$E_{SCI} := \left\{ \forall \mathbf{s} \in \mathcal{S} : \hat{B}_l(\mathbf{s}) \leq \mu(\mathbf{s}) \leq \hat{B}_u(\mathbf{s}) \right\}.$$

We want to show:

$$E_{SCI} \implies E.$$

Conditioning on the E_{SCI} event, assume for a fixed $\mathbf{s}' \in \mathcal{S}$, we have $\hat{B}_l(\mathbf{s}') \geq c$, then

$$\mu(\mathbf{s}') \geq \hat{B}_l(\mathbf{s}') \geq c$$

by E_{SCI} . This means that $\forall \mathbf{s} \in \mathcal{S} : \hat{B}_l(\mathbf{s}) \geq c$, we must also have $\mu(\mathbf{s}) \geq c$ holds as well, which is equivalent to the statement $\hat{B}_l^{-1}[c, +\infty) \subseteq \mu^{-1}[c, +\infty)$. \square

There are two issues with simply converting the lower band of SCI into inner confidence sets. The first major problem is that this inversion is conservative, as indicated by the coverage probability inequality in Proposition 1, and we do not know how conservative this construction is. In other words, is it possible to construct multiple confidence sets for different levels c and still maintain the type I error rate? And when will the equality hold? Second, this proposition only provides the inner confidence set as $B_l^{-1}[c, +\infty)$, but gives no outer confidence set. This is of interest because the outer confidence set would capture regions where the signal is not strong, and the region outside the outer confidence set would capture regions where $\mu(\mathbf{s}) < c$ with the desired probability. This is additional information not provided by the inner set or lower SCI. We address these issues together in the next section.

2.2.2 Simultaneous confidence sets for multiple inverse upper excursion sets

Improving on Proposition 1, we obtain equality in the coverage probability by introducing both upper and lower confidence sets for all levels in \mathbb{R} , as shown in Theorem 1.

Theorem 1. (Inverse upper excursion set) Let $\hat{B}_l(\mathbf{s})$ and $\hat{B}_u(\mathbf{s})$ be the pre-constructed SCIs on the domain \mathcal{S} , then

$$\mathbb{P} \left(\forall c \in \mathbb{R} : \hat{B}_l^{-1}[c, +\infty) \subseteq \mu^{-1}[c, +\infty) \subseteq \hat{B}_u^{-1}[c, +\infty) \right) = \mathbb{P} \left(\forall \mathbf{s} \in \mathcal{S} : \hat{B}_l(\mathbf{s}) \leq \mu(\mathbf{s}) \leq \hat{B}_u(\mathbf{s}) \right)$$

Proof. See appendix section. \square

Theorem 1 states that inner and outer confidence sets for all levels in the real line can be constructed based on the SCIs and maintain the same coverage probability as the SCIs. By introducing the outer confidence set in the probability statement in Proposition 1, the inversion will still be conservative for a single level c by Theorem 1. The detailed procedure is provided in Algorithm 1.

Algorithm 1 Simultaneous confidence sets for multiple inverse upper excursion sets

Require: α type I error rate SCI on the domain \mathcal{S} with lower band $\hat{B}_l(\mathbf{s})$ and upper band $\hat{B}_u(\mathbf{s})$.

Require: A discrete subset with m elements in $\mathbb{R} : \mathcal{C} = \{c_1, c_2, \dots, c_m\}$.

1: **for** c in \mathcal{C} **do**

2: Construct inner confidence set as $CS_{in}[c, +\infty) := \hat{B}_l^{-1}[c, +\infty) = \left\{ \mathbf{s} \in \mathcal{S} \mid \hat{B}_l(\mathbf{s}) \geq c \right\}$, and outer confidence set as $CS_{out}[c, +\infty) := \hat{B}_u^{-1}[c, +\infty) = \left\{ \mathbf{s} \in \mathcal{S} \mid \hat{B}_u(\mathbf{s}) \geq c \right\}$.

3: **end for**

4: **return** $CS_{in}[c, +\infty)$ and $CS_{out}[c, +\infty)$ for all $c \in \mathcal{C}$.

Remark. From the proof of Theorem 1 in the appendix, it can be seen that when \mathcal{C} is a strict subset of \mathbb{R} , as in Algorithm 1, the procedure is conservative, that is, it is guaranteed that $\mathbb{P}(\forall c \in \mathcal{C} : CS_{in}[c, +\infty) \subseteq \mu^{-1}[c, +\infty) \subseteq CS_{out}[c, +\infty]) > 1 - \alpha$. Only when $\mathcal{C} = \mathbb{R}$ the equality holds.

2.3 Estimating inverse lower excursion sets

We can define the *inverse lower excursion set*:

$$\mu^{-1}(-\infty, c] = \{ \mathbf{s} \in \mathcal{S} \mid \mu(\mathbf{s}) \leq c \} = \{ \mu^{-1}[c, +\infty) \}^C$$

where $\{ \mu^{-1}(-\infty, c] \}^C$ is the the closed complement of the inverse upper excursion set. We could not directly take the complement of the events in Theorem 1 to obtain the confidence sets for the inverse lower excursion set since there is an additional closure operation.

The following sets are defined as the outer and inner confidence sets for the inverse lower excursion set $\mu^{-1}(-\infty, c]$:

$$\text{CS}_{\text{in}}(-\infty, c] := \hat{B}_u^{-1}(-\infty, c] = \left\{ \mathbf{s} \in \mathcal{S} \mid \hat{B}_u(\mathbf{s}) \leq c \right\} = \{\hat{B}_u^{-1}[c, +\infty)\}^{\complement} = \{\text{CS}_{\text{out}}[c, +\infty)\}^{\complement} \quad (2.1)$$

$$\text{CS}_{\text{out}}(-\infty, c] := \hat{B}_l^{-1}(-\infty, c] = \left\{ \mathbf{s} \in \mathcal{S} \mid \hat{B}_l(\mathbf{s}) \leq c \right\} = \{\hat{B}_l^{-1}[c, +\infty)\}^{\complement} = \{\text{CS}_{\text{in}}[c, +\infty)\}^{\complement} \quad (2.2)$$

Lemma 1 in the Appendix shows that the two events, in which inverse upper or lower excursion sets for all $c \in \mathbb{R}$ are contained in the corresponding confidence sets, are equivalent. This directly leads to Corollary 1 below, which guarantees the coverage probability of the confidence sets for inverse lower excursion set.

Corollary 1. (Inverse lower excursion set) Let $\hat{B}_l(\mathbf{s})$ and $\hat{B}_u(\mathbf{s})$ be the pre-constructed SCIs on the domain \mathcal{S} , then

$$\mathbb{P} \left(\forall c \in \mathbb{R} : \hat{B}_u^{-1}(-\infty, c] \subseteq \mu^{-1}(-\infty, c] \subseteq \hat{B}_l^{-1}(-\infty, c] \right) = \mathbb{P} \left(\forall \mathbf{s} \in \mathcal{S} : \hat{B}_l(\mathbf{s}) \leq \mu(\mathbf{s}) \leq \hat{B}_u(\mathbf{s}) \right)$$

Proof. Using Lemma 1, we know that the following two events are equivalent

$$\begin{aligned} E_1 &= \left\{ \forall c \in \mathbb{R} : \hat{B}_l^{-1}[c, +\infty) \subseteq \mu^{-1}[c, +\infty) \subseteq \hat{B}_u^{-1}[c, +\infty) \right\} \\ E_2 &= \left\{ \forall c \in \mathbb{R} : \hat{B}_u^{-1}(-\infty, c] \subseteq \mu^{-1}(-\infty, c] \subseteq \hat{B}_l^{-1}(-\infty, c] \right\} \end{aligned}$$

From Theorem 1, the Corollary directly follows. \square

Remark. Observe that $\text{CS}_{\text{in}}(-\infty, c]$ is the region where we estimate the true mean is less than or equal to c with a pre-defined probability. From Equation 2.1, we know $\{\text{CS}_{\text{out}}[c, +\infty)\}^{\complement} = \text{CS}_{\text{in}}(-\infty, c]$. Therefore, instead of using confidence sets for inverse lower excursion set, $\text{CS}_{\text{in}}[c, +\infty)$ and $\{\text{CS}_{\text{out}}[c, +\infty)\}^{\complement}$ for inverse upper excursion set (Theorem 1) will be sufficient in finding the region where the true mean is greater or equal to c and the region where the true mean is less or equal to c respectively.

2.4 Estimating inverse interval sets

Another similar problem of interest is finding the set where the true mean is within a certain interval. For instance, a clinician may want to find patients with blood pressure that are within a certain healthy interval [48]. By taking the intersection of the upper inverse excursion set and lower inverse excursion set, we obtain the *inverse interval set* where $a < b \in \mathbb{R}$:

$$\mu^{-1}[a, b] := \{\mathbf{s} \in \mathcal{S} : a \leq \mu(\mathbf{s}) \leq b\} = \mu^{-1}[a, \infty) \cap \mu^{-1}(-\infty, b].$$

We define the following inner and outer confidence sets for the inverse interval set $\mu^{-1}[a, b]$:

$$\begin{aligned} \text{CS}_{\text{in}}[a, b] &:= \hat{B}_l^{-1}[a, \infty) \cap \hat{B}_u^{-1}(-\infty, b] = \{\mathbf{s} \in \mathcal{S} : \hat{B}_l(\mathbf{s}) \geq a \wedge \hat{B}_u(\mathbf{s}) \leq b\} \\ \text{CS}_{\text{out}}[a, b] &:= \hat{B}_u^{-1}[a, \infty) \cap \hat{B}_l^{-1}(-\infty, b] = \{\mathbf{s} \in \mathcal{S} : \hat{B}_u(\mathbf{s}) \geq a \wedge \hat{B}_l(\mathbf{s}) \leq b\}. \end{aligned}$$

To illustrate this in Figure 1, the true inverse interval set $\mu^{-1}[a, b]$, where $a = 0.2, b = 0.8$, is approximately located at $\{[0.02, 0.06] \cup [0.08, 0.11] \cup [0.27, 0.35]\}$ on the x-axis. The inner confidence set $\text{CS}_{\text{in}}[a, b]$ is located in the region on the x-axis by intersecting the red horizontal line at $y = 0.2$ with the uncolored horizontal dashed line at $y = 0.8$. The outer confidence set $\text{CS}_{\text{out}}[a, b]$ is located in the region by intersecting the colored (red, green or blue) horizontal lines at $y = 0.2$ with the complement of the red horizontal line at $y = 0.8$. Therefore, the inner confidence set is approximately located at $\{[0.03, 0.04] \cup [0.09, 0.10] \cup [0.29, 0.33]\}$ on the x-axis. And the outer confidence set is approximately located at $\{[0.01, 0.12] \cup [0.25, 0.36]\}$ on the x-axis.

Corollary 2 provides the theoretical guarantee for the coverage rate of the inner and outer confidence constructed for inverse interval sets.

Corollary 2. (Inverse interval set) Let $a < b \in \mathbb{R}$ and $\hat{B}_l(\mathbf{s})$ and $\hat{B}_u(\mathbf{s})$ be the pre-constructed SCIs on the domain \mathcal{S} , then

$$\begin{aligned} &\mathbb{P} \left(\forall a, b \in \mathbb{R}, a < b : \text{CS}_{\text{in}}[a, b] \subseteq \mu^{-1}[a, b] \subseteq \text{CS}_{\text{out}}[a, b] \right) \\ &= \mathbb{P} \left(\forall \mathbf{s} \in \mathcal{S} : \hat{B}_l(\mathbf{s}) \leq \mu(\mathbf{s}) \leq \hat{B}_u(\mathbf{s}) \right). \end{aligned}$$

Proof. This directly follows from Lemma 2 and Theorem 1. \square

Corollary 2 states that the confidence sets, constructed for all combinations of $a < b \in \mathbb{R}$, are guaranteed to have the same coverage rate as the SCIs. The algorithm for constructing confidence sets for inverse interval sets is shown in Algorithm 2.

Algorithm 2 Simultaneous confidence sets for multiple inverse interval sets

Require: α type I error rate SCIs on the domain \mathcal{S} with lower band $\hat{B}_l(s)$ and upper band $\hat{B}_u(s)$.

Require: $\mathcal{C} = \{(a_i, b_i) : i = 1, \dots, m, a_i < b_i\}$.

- 1: **for** (a, b) in \mathcal{C} **do**
- 2: Construct inner confidence set as $\text{CS}_{\text{in}}[a, b] := \hat{B}_l^{-1}[a, \infty) \cap \hat{B}_u^{-1}(-\infty, b]$, and outer confidence set as $\text{CS}_{\text{out}}[a, b] := \hat{B}_u^{-1}[a, \infty) \cap \hat{B}_l^{-1}(-\infty, b]$.
- 3: **end for**
- 4: **return** $\text{CS}_{\text{in}}[a, b]$ and $\text{CS}_{\text{out}}[a, b]$ for all $(a, b) \in \mathcal{C}$.

Using Corollary 2, the confidence sets produced are guaranteed to have the following probability statement hold with a finite level set $\mathcal{C} = \{(a_i, b_i) : i = 1, \dots, m, a_i < b_i\}$:

$$\mathbb{P}(\forall (a, b) \in \mathcal{C}, a < b : \text{CS}_{\text{in}}[a, b] \subseteq \mu^{-1}([a, b]) \subseteq \text{CS}_{\text{out}}[a, b]) > 1 - \alpha.$$

3 Simulations

All simulations are based on 5000 Monte Carlo independent realizations. First, we check the validity of our theorem and corollaries, and compare our method with [18] using continuous 1D and 2D dense functional data. Second, we focus on simulations of constructing confidence sets for inverse upper excursion sets in regression data cases, as these are more common in practice. Simulations for estimating inverse upper excursion sets of the mean function on a 2D grid of predictors using linear and logistic regression are conducted. Third, the discrete domain setting is demonstrated by constructing confidence sets for inverse upper excursion sets of coefficients in linear regression. We conclude with a comparison of the conservativeness of the coverage probabilities when constructing confidence sets for small number levels.

3.1 Dense functional data

We followed same setup as in [34] and generated functional signal-plus-noise 1D and 2D data:

$$(1\mathbf{D}) : Y(s) = \sin(8\pi s) \exp(-3s) + \frac{(0.6 - s)^2 + 1}{6} \cdot \frac{\mathbf{a}^T \mathbf{K}^A(s)}{\|\mathbf{K}^A(s)\|}, \quad s \in [0, 1]$$

$$(2\mathbf{D}) : Y(\mathbf{s}) = s_1 s_2 + \frac{s_1 + 1}{s_2^2 + 1} \cdot \frac{\mathbf{b}^T \mathbf{K}^B(\mathbf{s})}{\|\mathbf{K}^B(\mathbf{s})\|}, \quad \mathbf{s} = (s_1, s_2) \in [0, 1]^2$$

with $\mathbf{a} \sim \mathcal{N}(0, I_{7 \times 7})$ and $\mathbf{b} \sim \mathcal{N}(0, I_{36 \times 36})$. The vector $\mathbf{K}^A(s)$ has entries $K_i^A(s) = \binom{6}{i} s^i (1 - s)^{6-i}$, the $(i, 6)$ th Bernstein polynomial for $i = 0, \dots, 6$ and $\mathbf{K}^B(\mathbf{s})$ is the vector of all entries from the 6×6 -matrix $K_{ij}(\mathbf{s}) = \exp\left(-\frac{\|\mathbf{s} - \mathbf{x}_{ij}\|^2}{2h^2}\right)$ with $\mathbf{x}_{ij} = (i, j)/6$ and $h = 0.06$. Examples of sample paths of the signal-plus-noise models and the error fields can be found in [34]. Figures 1 and 3 display the true mean function over the space of support, where the 1D functional data was sampled from the corresponding model on an equidistant grid of 200 points of $[0, 1]$, and the 2D functional data was simulated on an equidistant grid with 50 points in each dimension. The SCIs were generated through a multiplier bootstrap procedure whose details can be found in [34] Appendix A. Once we have the SCIs, confidence sets are directly obtained by inversion.

Figure 1 displays 1D simulated data when the sample size is $N = 20$ at each grid point for one realization. Figure 3 shows 2D simulated data for one realization of the confidence sets when the sample size is $N = 50$. If the researcher wants to find the region where the true mean is greater than or equal to 0.3, 0.5 and 0.7, then the most right plot in the first row of Figure 3 will be useful. If the researcher wants to find the region where the true mean is greater or equal to 0.3 (inside the red contour line) and less than 0.3 (outside the blue contour line) with 95% confidence, it would be helpful to investigate the most left panel of the second row of Figure 3.

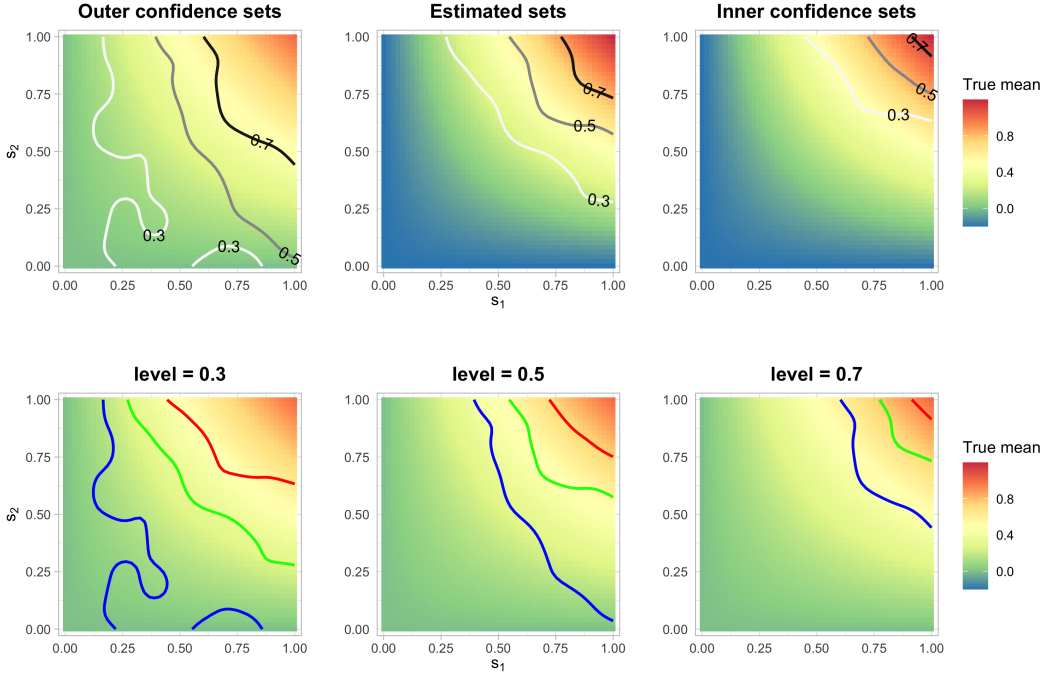


Figure 3: 2D dense functional data simulation showcase. The first row displays the contours of the confidence sets in one single plot for the outer confidence sets, estimated inverse set and inner confidence sets, respectively. The three plots in the second row display the contours of the confidence sets for where the true mean is greater or equal to the individual level 0.3, 0.5 or 0.7 respectively. The blue line is the contour of the outer confidence set, the green line is the contour of the estimated inverse set and the red line is the contour of the inner confidence set.

Table 1: Simulation coverage rate for 1D and 2D dense functional data.

N	1D				2D			
	SCI	Upper	Lower	Interval	SCI	Upper	Lower	Interval
10	94.98	95.00	95.00	95.18	95.16	95.16	95.18	95.32
20	94.94	95.00	95.00	95.22	95.96	95.96	96.06	96.42
30	95.26	95.34	95.34	95.54	94.92	94.96	94.96	95.40
50	95.02	95.10	95.10	95.40	94.92	94.98	94.98	95.42
100	94.94	94.98	94.98	95.58	94.88	94.90	94.96	95.46
150	94.58	94.64	94.64	95.06	95.10	95.12	95.18	95.64

The simulation standard error is 0.006, calculated as the standard error of a Bernoulli random variable with $p = 0.95$ divided by $\sqrt{5000}$ where 5000 is the number of Monte Carlo simulations.

In Table 1, we demonstrate the validity of Theorem 1 (labeled as Upper in the table), Corollary 1 (Lower) and Corollary 2 (Interval). The SCI coverage rate is calculated as the percentage of simulation instances such that the true means for each grid point are contained in the corresponding confidence intervals. The coverage rates for the confidence sets are defined as the percentage of simulation instances such that the inner confidence set is contained in the true inverse set, and the true inverse set is contained in the outer confidence set for every pre-defined level c . For inverse upper and lower excursion sets, we checked the containment of confidence sets over 5000 equidistant levels c across the range of minimum and maximum of the true mean function. For the inverse interval set, we checked on the set of intervals (a, b) where a and b are sampled at a step size of 0.005 ranging from the minimum to the maximum of the true mean, forming a grid with the condition $a < b$. From Table 1, we can see that the coverage rates of the different types of confidence sets were almost exactly the same as the SCI regardless of the sample size for both 1D and 2D dense functional data with the predefined number of levels, validating our theory.

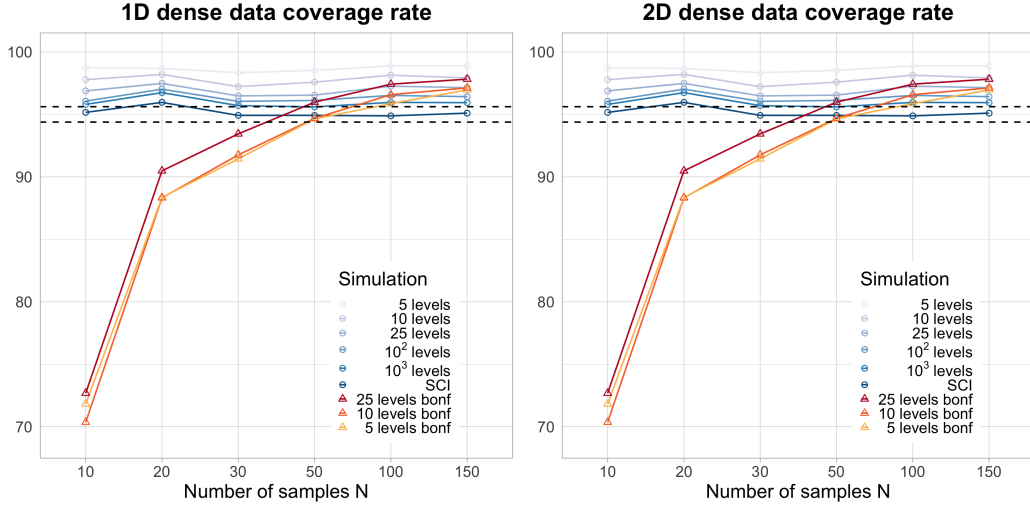


Figure 4: Dense functional data simulation: coverage rate of confidence sets for different number of levels for inverse upper excursion sets. The dashed black line is 95% plus or minus twice the standard error for a Bernoulli random variable with $p = 0.95$ divided by $\sqrt{5000}$.

In addition, we checked the conservativeness of the simultaneous confidence set over a different number of levels for inverse upper excursion sets, and the results are displayed in Figure 4. As the number of levels decreases, the coverage rate increases, and it depends on the coverage rate of SCI at the corresponding sample size for the realized 5000 simulations. For example, the coverage rate of SCI at sample size 20 for 2D data was 95.96%, which leads to a higher coverage rate of 96.74% for 1000 levels and 97.32% for 50 levels. As the number of confidence sets decreased to 5, the coverage rate rose to around 98% for both 1D and 2D dense functional data. We also compared our method with the asymptotic single-level confidence sets [18], adjusted for multiple levels by using Bonferroni adjustments for every single level. Figure 4 shows that the Bonferroni adjusted multiple single level confidence sets yield coverage lower than the nominal level at small sample sizes and produced higher coverage at larger sample sizes. This is expected since this single-level method is only valid asymptotically for a single level when the sample size is large and becomes conservative when adjusted for multiple levels using Bonferroni adjustment.

3.2 Regression outcome excursion sets estimation

We have generated linear and logistic regression data using the following models,

$$(\text{Linear}) : y_i = \beta_0 + \beta_1 x_{i1} + \beta_2 x_{i1}^2 + \beta_3 x_{i1}^3 + \beta_4 x_{i2} + \beta_5 x_{i2}^2 + \beta_6 x_{i2}^3 + \epsilon_i \quad (3.1)$$

$$(\text{Logistic}) : \log\left(\frac{p_i}{1 - p_i}\right) = \beta_0 + \beta_1 x_{i1} + \beta_2 x_{i1}^2 + \beta_3 x_{i1}^3 + \beta_4 x_{i2} + \beta_5 x_{i2}^2 + \beta_6 x_{i2}^3, \quad (3.2)$$

where $i = 1, \dots, N$ denote the index for subjects and N for training sample size, $\beta = (\beta_0, \beta_1, \beta_2, \beta_3, \beta_4, \beta_5, \beta_6) = (-1, 1, 0.5, -1.1, -0.5, 0.8, -1.1)$, the error $\epsilon_i \stackrel{i.i.d.}{\sim} N(0, 2)$ and p_i denotes the probability of $y_i = 1$ for the logistic regression model. The predictors for training the model $\mathbf{x}_i = (1, x_{i1}, x_{i1}^2, x_{i1}^3, x_{i2}, x_{i2}^2, x_{i2}^3)^T$ are generated from two independent standard normal distributions for x_{i1} and x_{i2} , and we denote the design matrix of the training data as $\mathbf{X} = (\mathbf{x}_1, \dots, \mathbf{x}_n)^T$. The predictions are made on an equidistant grid of 100 points on the interval $[-1, 1]$ for the two predictors. We denote by $\tilde{\mathbf{X}}$ the design matrix for the prediction grid, which can also be called the test data design matrix. For our simulation setup, $\tilde{\mathbf{X}}$ is a 10,000 by 7 matrix since for each dimension we have 100 points spanning from -1 to 1. Note that the rows of $\tilde{\mathbf{X}}$ are equivalent to \mathbf{s} in the Theory section 2.

To generate SCI for the mean outcome on the prediction data grid, we implemented non-parametric bootstrap. Compared to other bootstrap methods, the non-parametric bootstrap method requires fewer assumptions. Other methods such as using the Gaussian Kinematic formula for constructing SCI [34] are available as well. We introduce a linear function $f(\beta, \mathbf{X})$ that takes in the coefficients vector and design matrix and returns a vector with the same length as the number of rows of \mathbf{X} . For our simulation setup, this linear function are the equations 3.1 and 3.2 without the errors. The generation process for SCIs of the linear regression mean function is detailed in Algorithm 3.

Algorithm 3 SCI for the mean outcome of regression on a fixed test design matrix

Require: Training data outcome \mathbf{y} and design matrix \mathbf{X} . Test design matrix $\tilde{\mathbf{X}}$.
Require: Number of Bootstraps L and a fixed function $f(\boldsymbol{\beta}, \mathbf{X})$, empty vector \mathbf{r}^{max} .

- 1: Obtain $\hat{\boldsymbol{\beta}}$ fitted on the training data \mathbf{y} and \mathbf{X} using least squares.
- 2: Calculate the estimated mean outcome vector on the test design matrix (prediction grid) $\hat{E}(\tilde{\mathbf{y}}) := f(\hat{\boldsymbol{\beta}}, \tilde{\mathbf{X}})$ and the estimated standard deviation $\hat{\sigma}$ of $\hat{E}(\tilde{\mathbf{y}})$. For linear regression, this is the estimated mean outcome on the same scale as \mathbf{y} , whereas for generalized linear regression, $\hat{E}(\tilde{\mathbf{y}})$ is the estimated linear mean outcome before taking the transformation.
- 3: **for** b in $1 : L$ **do**
- 4: Resample with replacement on the training data set: $\mathbf{y}_b, \mathbf{X}_b$.
- 5: Fit the model on the resampled training data $\mathbf{y}_b, \mathbf{X}_b$, and obtain $\hat{\boldsymbol{\beta}}_b$.
- 6: Calculate the vector for the estimated mean $\hat{E}(\tilde{\mathbf{y}}_b) := f(\hat{\boldsymbol{\beta}}_b, \tilde{\mathbf{X}})$ and the standard deviation $\hat{\sigma}_b$ for every point in the prediction grid.
- 7: Calculate the vector of standardized absolute residual vector for every sample in the test design matrix $\mathbf{r}_b = \frac{|\hat{E}(\tilde{\mathbf{y}}_b) - \hat{E}(\tilde{\mathbf{y}})|}{\hat{\sigma}_b}$. Append the max element of \mathbf{r}_b to \mathbf{r}^{max} .
- 8: **end for**
- 9: Take the $1 - \alpha$ quantile over the empirical distribution generated by \mathbf{r}^{max} as our threshold a .
- 10: **return** SCI on the test design matrix (prediction grid) as $(\hat{E}(\tilde{\mathbf{y}}) - a \times \hat{\sigma}, \hat{E}(\tilde{\mathbf{y}}) + a \times \hat{\sigma})$. For generalized linear regression, transform the SCI back to the data scale using the monotone link function.

Figures 5 and 6 display the regression true mean 2D plot with the estimated confidence set contour lines overlaid on top when the training sample size is $N = 500$. The outer confidence set, estimated inverse sets and inner confidence sets for all levels are displayed in the first row three plots, and each plot in the second row displays the outer, estimated and inner sets all at once in a single plot for each level. For example, first row and third column of Figure 5 displays the estimated inner confidence sets for level $-1, -0.5$ and 0 simultaneously. For any value of $-1 < x_1 < 1$ and $-1 < x_2 < -0.75$, the true mean of the linear function conditioned on the two predictors is greater than 0 with at least 95% confidence. In Figure 6 second row and second column, we can see that for any value of $x_1 > 0$ and $x_2 > 0.9$, we have at least 95% confidence that the true probability of classifying $y = 1$ is greater than 50%, which is where the inner confidence set for level 0.5 is. We also know that if $-0.8 < x_1 < 0$ and $x_2 > -0.4$, then we have at least 95% confidence that the true probability is less than 50% of classifying $y = 1$, which is the region outside the outer confidence set (blue line). This is a much more intuitive interpretation of the predictors' effect than just interpreting coefficients.

In Figure 7, we displayed the coverage rate for different numbers of levels for both the linear and logistic regression. The coverage rate for 5 levels increased only around 1% for linear regression and around 2% for logistic regression compared to SCI coverage rate. This is due to the high correlation between the estimated means in the prediction grid, which we address in section 3.4.

3.3 Regression coefficient excursion sets estimation

This simulation for regression coefficients demonstrates the validity of confidence sets on discrete domain by using the SCI for coefficients in linear regression. To flexibly control the number of coefficients, we generated the data under the following model:

$$y_i = \beta_0 + \sum_{j=1}^{M-1} \beta_j x_{ij} + \epsilon_i$$

where $\boldsymbol{\beta} = (\beta_0, \beta_1, \dots, \beta_{M-1}) \sim N(\mathbf{0}, \mathbf{I})$ are generated once and fixed for all simulations instances, $\mathbf{x}_i = (x_{i1}, x_{i2}, \dots, x_{i,M-1}) \sim N(\mathbf{0}, \boldsymbol{\Sigma})$ are generated randomly for every new simulation instances, and $\boldsymbol{\Sigma}$ is a auto-regressive covariance matrix with an order of 1, decay factor $\rho = 0.4$ and variance of 1 on the diagonal. The irreducible error ϵ_i follows an independent standard normal. The SCIs of the coefficients were generated similarly to the regression outcome SCI by using non-parametric bootstrapping as shown in Algorithm 3.

Figure 8 shows the confidence sets estimation for the 50 coefficients in one realization of the simulations when $N = 500$. The red points are the inner confidence sets for each level which are contained in the true inverse upper excursion sets (green + red points) that are contained in the outer confidence set (blue+green+red points).

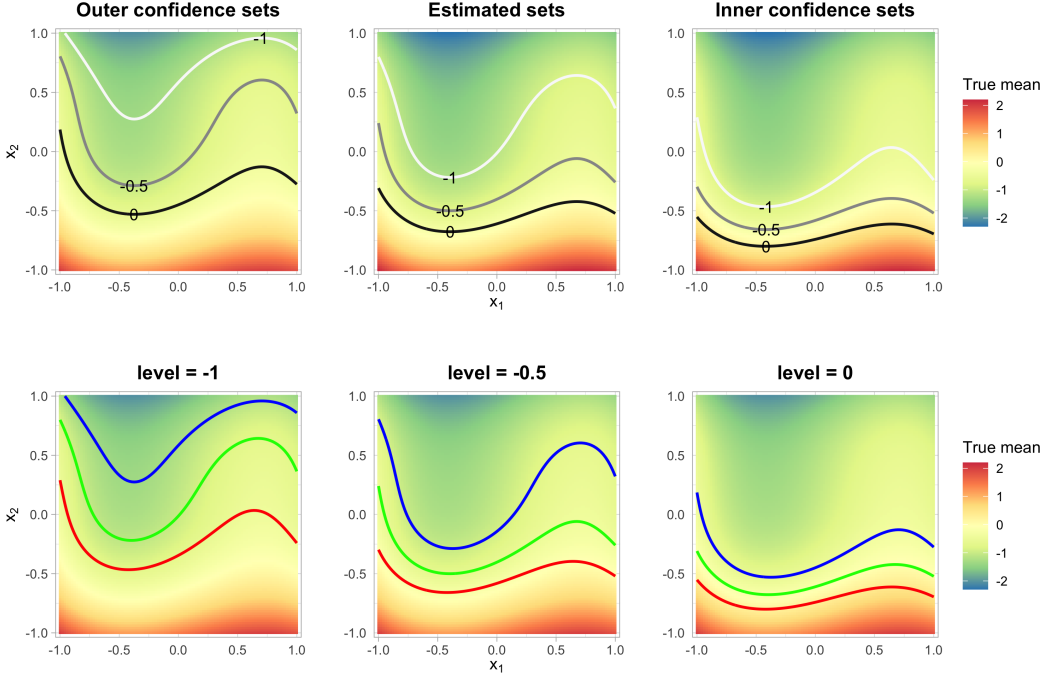


Figure 5: Confidence sets for linear regression predicted mean estimators on a 2D grid. The first row displays the contours of the three levels in one single plot for the outer confidence sets, estimated inverse upper excursion set and the inner confidence sets, respectively. The three plots in the second row display the confidence sets for where the true mean is greater or equal to the individual level -1 , -0.5 or 0 respectively. The blue line is the contour of the outer confidence set, the green line is the contour of the estimated inverse set and the red line is the contour of the inner confidence set. The predictions are made on a grid of equidistant grid of 100 points on $[-1, 1]$.

We investigated how the coverage rate changes with both sample size and the number of coefficients in the model for different number of levels. As shown in Figure 9, the coverage rates for a small number of levels are more conservative than both the dense functional and regression outcome model and do not vary with either the number of coefficients or the number of samples. The SCI coverage rate failed to be in the nominal range when the sample size to the number of coefficient ratio is small due to the instability when fitting the model with the bootstrapped data. The overall conservativeness for the finite number of levels is due to the low correlation between the estimated coefficients as discussed in Section 3.4.

3.4 Conservativeness of confidence sets depends on correlations of the estimators

This section investigates how the coverage probability of confidence sets for a finite number of levels changes with the correlations between the estimator $\hat{\mu}(s)$ in the domain \mathcal{S} . In Figure 10, we displayed the pairwise absolute correlation density of the estimators for the simulation setup as shown in Figures 5, 6, and 8 for linear grid prediction means, logistic grid prediction means and discrete coefficients. For example, the green line shows the density for the correlations between every pair of the mean predictions in the grids for linear regression in one simulation instance. We can see most pairs of the discrete coefficient estimates have low absolute correlation at around 0.10, whereas the linear regression grid prediction means estimators' absolute correlations concentrates at around 0.75 leading to the least conservative coverage for finite levels of confidence sets. The logistic regression prediction mean estimators' absolute correlations are less concentrated at higher values and thus they produce more conservative coverage than the linear regression even though both the linear and logistic models are generated with the same underlying linear model.

An enlightening example in the linear regression setting demonstrates that the conservativeness is more dependent on the correlations of the estimators instead of the number of the estimators that confidence sets are constructed for. The correlation matrix of the coefficient estimators is:

$$\text{cov}(\hat{\beta}) = \sigma^2 (\mathbf{X}' \mathbf{X})^{-1}$$

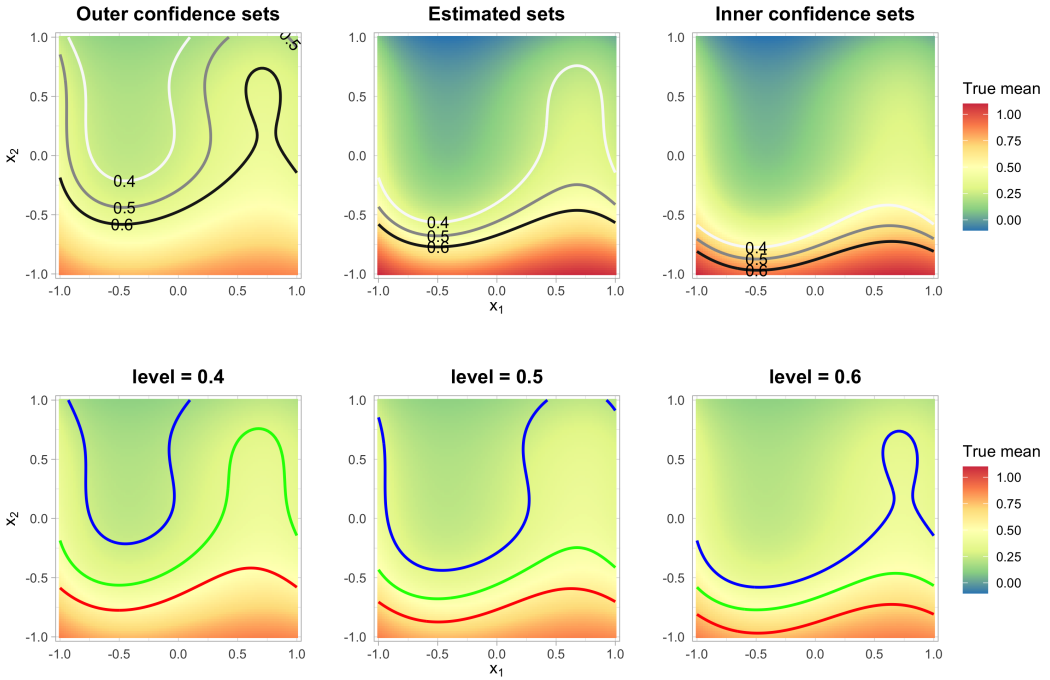


Figure 6: Confidence sets for logistic regression predicted mean estimator for probability on a 2D grid. The first row displays the contours of the three levels in one single plot for the outer confidence sets, estimated inverse upper excursion set and the inner confidence sets, respectively. The three plots in the second row display the confidence sets for where the true mean is greater or equal to the individual level 0.4, 0.5 or 0.6 respectively. The blue line is the contour of the outer confidence set, the green line is the contour of the estimated inverse set and the red line is the contour of the inner confidence set. The predictions are made on a grid of equidistant grid of 100 points on $[-1, 1]$.

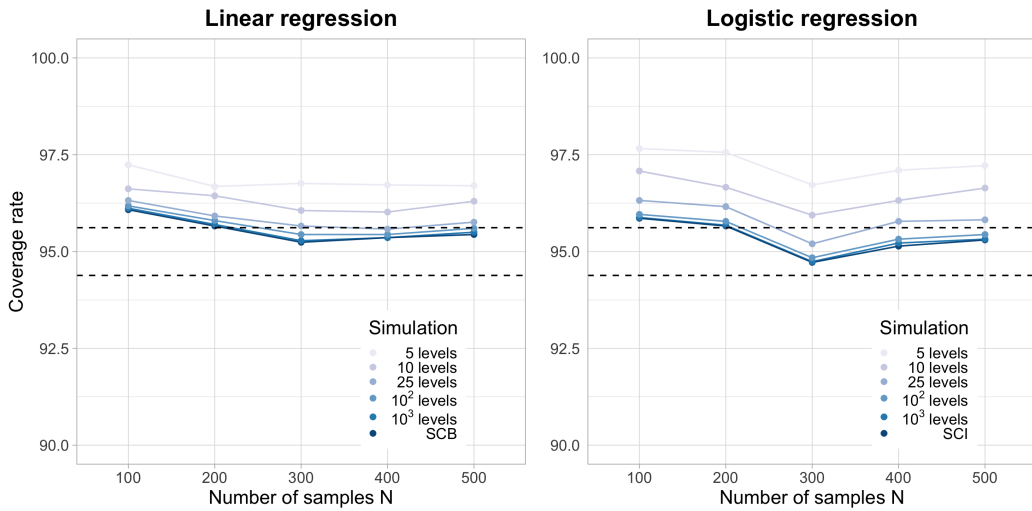


Figure 7: Regression outcome simulation confidence sets coverage rate for different number of levels for inverse upper excursion sets. The dashed black line is 95% plus or minus twice the standard error for a Bernoulli random variable with $p = 0.95$ divided by $\sqrt{5000}$.

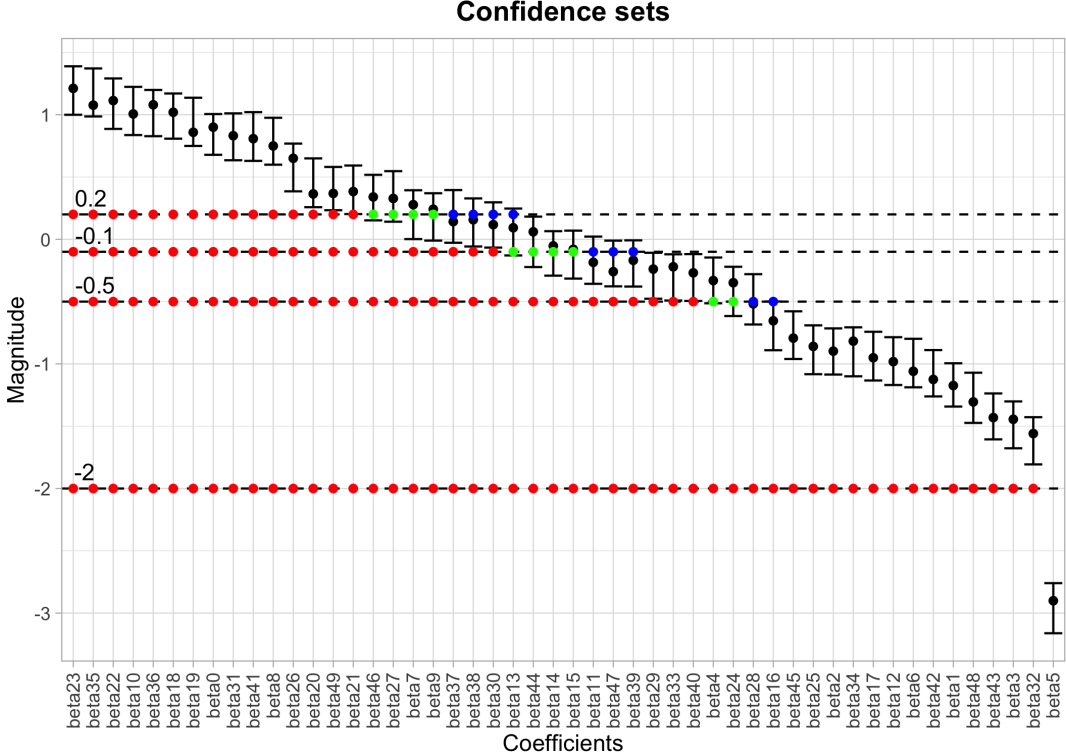


Figure 8: Confidence sets for inverse upper excursion sets of coefficients in the discrete linear regression example. The black points indicate the true means ordered by the lower interval values from left to right. For each level, the red points indicate the inner confidence sets, which are contained in the true inverse upper excursion sets (green+red points) that are contained in the outer confidence set (blue+green+red points).

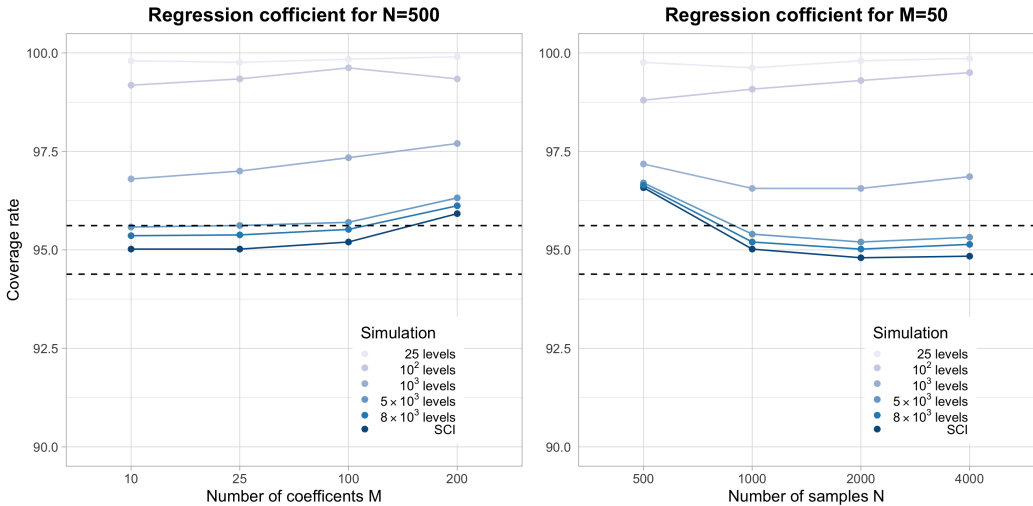


Figure 9: Regression coefficient simulation confidence sets coverage rate for different number of levels for inverse upper excursion sets. The dashed black line is $95\% \pm \text{twice the standard error}$ for a Bernoulli random variable with $p = 0.95$ divided by $\sqrt{5000}$.

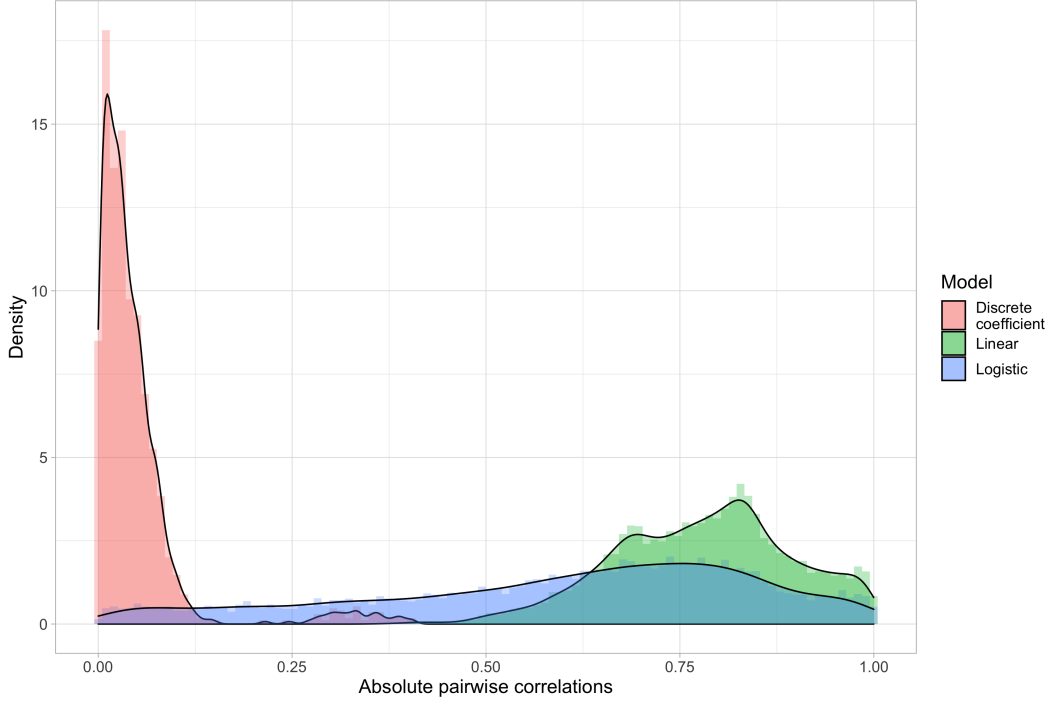


Figure 10: Absolute pairwise correlations of the estimators for different models

Table 2: Simulation coverage rates for fix grid step size for linear regression model set up as shown in Equation 3.1.

# of grid points	5 levels	25 levels	100 levels	1000 levels	SCI
5	95.70	95.48	95.26	95.16	95.16
10	95.28	94.88	94.80	94.66	94.62
20	95.96	95.38	95.20	95.08	95.06
50	95.82	95.14	94.98	94.94	94.94
80	96.50	95.40	95.36	95.20	95.18

The simulation standard error is 0.006, calculated as the standard error of Bernoulli random variable with $p = 0.95$ divided by $\sqrt{5000}$ where 5000 is the number of Monte Carlo simulations.

where σ^2 is the error variance and \mathbf{X} is the training design matrix. Then, the pairwise correlation between the mean estimator \hat{y}_i and \hat{y}_j for the two points \mathbf{x}_i and \mathbf{x}_j in the testing grid is:

$$\text{cor}(\hat{y}_i, \hat{y}_j) = \frac{\mathbf{x}_i(\mathbf{X}'\mathbf{X})^{-1}\mathbf{x}_j'}{\sqrt{\mathbf{x}_i(\mathbf{X}'\mathbf{X})^{-1}\mathbf{x}_i'}\sqrt{\mathbf{x}_j(\mathbf{X}'\mathbf{X})^{-1}\mathbf{x}_j'}} \quad (3.3)$$

If \mathbf{x}_i and \mathbf{x}_j are close in Euclidean distance, then the correlation of the prediction mean estimator would be extremely close to 1 regardless of the correlation of the coefficients $\text{cov}(\hat{\beta}) = \sigma^2(\mathbf{X}'\mathbf{X})^{-1}$. This is because the multiplication of the two square roots in the denominator would have similar value as the numerator in Equation 3.3. We constructed linear regression outcome simulations under the same model setup as above but with the step size of 0.02 between the prediction grid points and only vary the number of grid points for a fixed fitting data sample size of 300. For example, for 5 grid prediction points in one dimension, the grid points would be (-0.04,-0.02,0,0.02,0.04). As the number of grid points increases to 100, that would be the same simulation setup in section 3.2, thus we omit it from this simulation setup. Table 2 illustrates that if the points are closer together (thus high correlated), the coverage rate of the confidence sets for finite levels would be close to the coverage rate for SCIs regardless of the number of estimators we are constructing.

4 Applications

4.1 Excursion set maps for climate data

With global warming emerging as a serious worldwide environmental issue, it is of interest to assess which geographical regions are particularly at high risk of an increase in temperature. Two sets of 29 spatially registered arrays of mean summer temperatures (June-August) produced by the WRFG climate model as part of the North American Regional Climate Change Assessment Program (NARCCAP) project [49, 50] are given at a fine grid of fixed locations 0.5 degrees apart in geographic longitude and latitude over North America over two time periods: late-20th century (1971–1999) and mid-21st century (2041–2069). Here we consider the problem of determining which regions have a mean difference in temperature greater than a certain value between the two time periods for summer. This value was set to be 2°C in [51, 52, 18], but the value is rather arbitrary. Why would a difference of 1°C or even 4°C not be of greater importance? The purpose of the analysis presented here is to show how more excursion thresholds can be explored without losing error control.

We followed the same modeling method approach as in [18]. Briefly, we consider a point-wise linear model with an auto-regressive (AR1) correlation structure for the correlation between different years within every grid point (location):

$$\begin{aligned} Y_j(\mathbf{s}) &= T^{(a)}(\mathbf{s}) + m^{(a)}(\mathbf{s})t_j^{(a)} + \epsilon_j(\mathbf{s}), \quad j = 1, \dots, n^{(a)} \\ Y_j(\mathbf{s}) &= T^{(b)}(\mathbf{s}) + m^{(b)}(\mathbf{s})t_j^{(b)} + \epsilon_j(\mathbf{s}), \quad j = n^{(a)} + 1, \dots, n^{(a)} + n^{(b)} \end{aligned}$$

where $n^{(a)} = n^{(b)} = 29$ are the number of years within the "past" and "future" periods. Here t_j is the year number normalized to have mean 0 within each "past" and "future" periods, and the model coefficients are $T(\mathbf{s})$ and $m(\mathbf{s})$. Our main interest is to estimate the difference $T^{(b)}(\mathbf{s}) - T^{(a)}(\mathbf{s})$. The 90% SCIs were obtained through multiplier bootstrap which accounted the correlations between different locations. For more details, please refer to [18].

In the first row of Figure 2, we display the point estimate of inverse upper excursion set, outer and inner confidence sets of temperature difference 1, 1.5, 2, 2.5 and 3 Celsius. For example, we are at least 90% confident that most of the United States and the northern part of Mexico have a summer temperature difference less than 3°C as seen in the outer confidence set plot. On the other hand, we are at least 90% confident that the Rocky Mountains and the Sierra Madre Occidental mountains of Mexico are at risk of exhibiting warming of 2°C or more in the given time period which can be seen in the inner confidence set plot.

We also compare our simultaneous finite sample method to the asymptotic single level confidence set in [18] using the same data at a temperature difference of 2°C . Taking the ratio of the SCI quantiles (the value a in Algorithm 3) calculated from the multiplier bootstrap for the two methods (single level confidence set used a subset of the support for multiplier bootstrap whereas simultaneous confidence used all the points on the support for bootstrap), the simultaneous confidence set threshold is around 127% (3.8/3) larger than single-level confidence set's threshold value. The position and size of the outer and inner confidence set from the two methods do not differ substantially which can be observed by comparing the level = 2°C plot in Figure 2 with Figure 1 in [18]. This leads to a similar interpretation of the results.

4.2 Prediction uncertainty quantification for severe outcome of COVID and non-COVID patients

Coronavirus disease 2019 (COVID-19) has caused significant morbidity and mortality worldwide. Statin medications used by cardiovascular disease (CVD) patients may have a protective effect against severe COVID due to their anti-inflammatory effects [53]. [54] performed a retrospective single-center study of all patients hospitalized at University of California San Diego Health between February 10, 2020 and June 17, 2020 ($n = 170$ hospitalized for COVID-19, $n = 5,281$ COVID-negative controls). Here we will use the same data and a similar multivariate logistic regression model to showcase our confidence set method. For more details of the data, please refer to [54].

The binary outcome of interest is severe outcome of the admitted patient, defined as either admission to the intensive care unit (ICU) or death. The main predictor is whether the patient is taking statin medications or not, and we have adjusted for potential confounders such as angiotensin-converting enzyme (ACE) inhibitors, angiotensin II receptor blockers (ARB), sex, age at diagnosis, chronic kidney disease (CKD), hypertension, cardiovascular disease (CVD), diabetes and obesity. Instead of only investigating the main effect of statin in the COVID positive patients, we pooled the COVID negative and positive population (total sample size of $n = 5451$) and added an interaction term between COVID positive indicator and statin medication in the logistic regression model. That is, the log odds of the severe outcome are modeled as a linear function of statin, COVID positive indicator, the interaction between the two, and the remaining confounders.

The use of statin [adjusted odds ratio (aOR) 0.78, confidence interval (CI) 0.66 to 0.93] is associated with decreased probability of severe outcome, whereas COVID indicator (aOR 4.08, CI 2.82 to 5.95) was associated with an increased

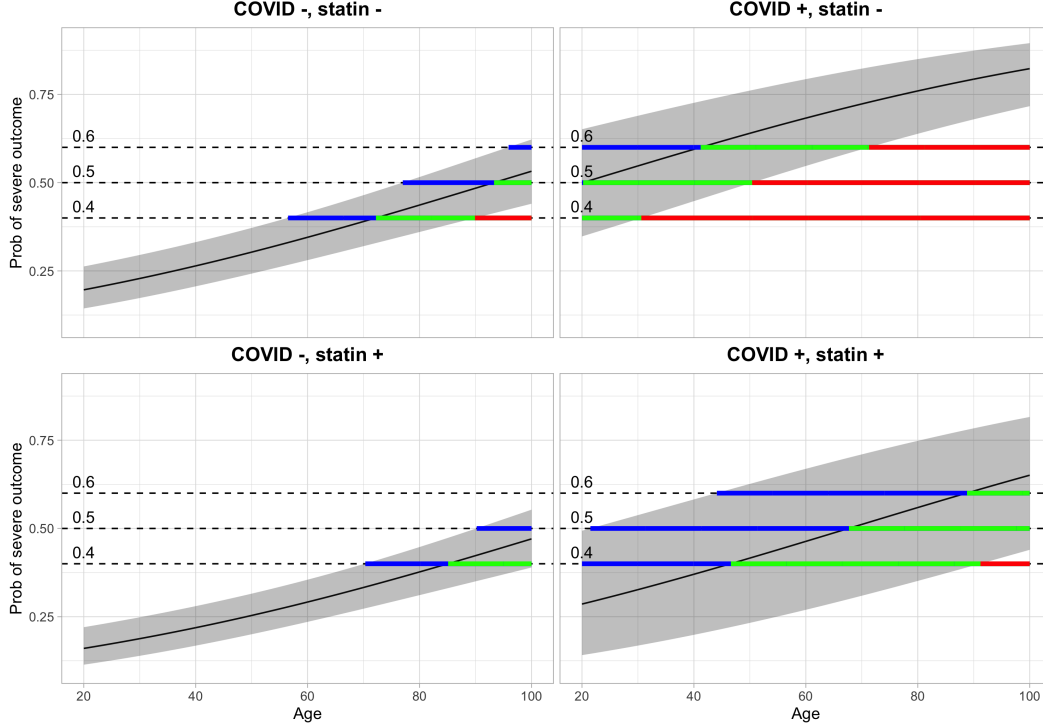


Figure 11: Simultaneous confidence set for the probability of severe outcome. We fixed other variables at ACE = 0, ARB = 0, sex = Male, CKD = 1, hypertension=1, CVD = 1, diabetes=1, obesity = 1. The gray shaded area is the 95% SCIs, the solid black line is the estimated probability. The red horizontal line shows the inner confidence sets (where the lower SCIs are greater than the corresponding level) which are contained in the estimated inverse upper excursion set colored as the green and red horizontal line (where the estimated means are greater than the corresponding levels); the outer confidence sets are colored by the blue, green and red line (where the upper SCIs are greater than the corresponding levels) and contain both the estimated inverse sets and the inner confidence sets.

probability of severe outcome, and the interaction term for COVID indicator and use of statin was marginally significant (aOR 0.51, 0.25 to 1.05) meaning that statin was more protective in the COVID positive patients. Age at diagnosis was a notable contributor to severe outcome with 2% (CI 1% to 3%) increase in the adjusted odds ratio for one year increase of age at diagnosis.

We constructed confidence sets for inverse upper excursion sets of three levels of severe outcome probability 0.4, 0.5 and 0.6 on the continuous prediction grid of age spanning from 20 to 100 with a step size of 0.1, and on the discrete prediction grid of COVID positive or not and whether taking statin or not, as shown in Figure 11. We fixed other variables at ACE = 0, ARB = 0, sex = Male, CKD = 1, hypertension=1, CVD = 1, diabetes=1, obesity = 1. We use Algorithm 3 to construct the SCIs for the probability of severe outcome on the prediction grid. Then, the corresponding three confidence sets are built and demonstrated in Figure 11. If any patient's characteristic falls within the red solid line, the probability of severe disease will be higher than the corresponding level, whereas if any patient's characteristic falls outside the colored (blue+green+red) solid line, the probability of severe disease will be lower than the corresponding level. These assertions hold for all levels and grid points simultaneously with 95% confidence, or 5% probability of making any mistakes, assuming that the model is correct. For example, we are confident that patients whose age is from 40 to 60 with COVID and not taking statin (Figure 11, top right, red set) will have a higher than 40% probability of getting severe outcome, whereas the same aged patients without COVID and taking statin (Figure 11, bottom left, outside of blue set) will have less than 40% probability, conditioned on the other variables at the fixed values.

5 Discussion

We have introduced an innovative concept of inverse set estimation and proposed inversion of SCIs as a way to construct simultaneous confidence sets for quantifying the uncertainty in estimating the inverse set. Previously, inverse set estimation methods have often been limited to data supported on a continuous domain such as dense functional spatial

data. We demonstrated that inverse set estimations can be used and provide insightful inference in other continuous or discrete data scenarios such as regression prediction and finding the coefficients with values greater than certain threshold levels.

In addition, our simultaneous confidence set method solved the dilemma of which level to choose for the inverse set. This is especially important since there is often no universal consensus on which threshold level to apply, even within a well-defined problem. Our construction allows the analyst to choose the excursion level freely, without concern for inflating the error rate. This comes with the drawback that our method is conservative when applied to a small number of excursion levels. However, we empirically demonstrated that this conservativeness depends on the specific model and data. For confidence sets of linear regression predictions, the type I error is very close to the nominal 5% with only 5 levels in the simulation study. Furthermore, if a slight decrease in power is not of great importance, our simultaneous method outshines the single-level method in three major aspects: our method is not asymptotic and valid for finite samples, produces valid confidence sets for multiple levels, and can be widely applicable to different kinds of data.

The potential of our method is not fully explored, since it is possible to apply our method to other statistical procedures that output SCIs. Confidence sets can be built by inverting the SCIs without additional assumptions or computational costs for these methods. This will aid inference and interpretation in applications such as survival analysis [42], longitudinal data analysis [36] and genetic SNP effect analysis [37, 39, 38].

A Proofs

A.1 Theorem 1

Proof. From the definition of inner confidence set, outer confidence set and inverse set, the first equality follows:

$$\begin{aligned} & \mathbb{P}\left(\forall c \in \mathbb{R} : \hat{B}_l^{-1}(U_c) \subseteq \mu^{-1}(U_c) \subseteq \hat{B}_u^{-1}(U_c)\right) \\ &= \mathbb{P}\left(\forall c \in \mathbb{R} : \left(\{\hat{B}_l(\mathbf{s}) \geq c\} \subseteq \{\mu(\mathbf{s}) \geq c\}\right) \wedge \left(\{\mu(\mathbf{s}) \geq c\} \subseteq \{\hat{B}_u(\mathbf{s}) \geq c\}\right)\right) \\ &= \mathbb{P}\left(\forall \mathbf{s} \in \mathcal{S} : \hat{B}_l(\mathbf{s}) \leq \mu(\mathbf{s}) \leq \hat{B}_u(\mathbf{s})\right). \end{aligned}$$

To show the second equality, we need to show that the following two events are equivalent:

$$\begin{aligned} E_1 &= \left\{ \forall c \in \mathbb{R} : \left(\{\hat{B}_l(\mathbf{s}) \geq c\} \subseteq \{\mu(\mathbf{s}) \geq c\}\right) \wedge \left(\{\mu(\mathbf{s}) \geq c\} \subseteq \{\hat{B}_u(\mathbf{s}) \geq c\}\right) \right\} \\ E_2 &= \left\{ \forall \mathbf{s} \in \mathcal{S} : \mu(\mathbf{s}) \geq \hat{B}_l(\mathbf{s}) \wedge \mu(\mathbf{s}) \leq \hat{B}_u(\mathbf{s}) \right\} \end{aligned}$$

First, let's show E_2 implies E_1 . Assume E_2 happened, then for any fixed $c \in \mathbb{R}$,

$\forall \mathbf{s} \in \mathcal{S}$ such that $\hat{B}_l(\mathbf{s}) \geq c$, then $\mu(\mathbf{s}) \geq \hat{B}_l(\mathbf{s}) \geq c$,

$\forall \mathbf{s} \in \mathcal{S}$ such that $\mu(\mathbf{s}) \geq c$, then $\hat{B}_u(\mathbf{s}) \geq \mu(\mathbf{s}) \geq c$.

Second, let's show E_1 implies E_2 . Proof by contradiction. Assume E_1 happened and $\exists \mathbf{s}' \in \mathcal{S}$ s.t.

$$\hat{B}_l(\mathbf{s}') > \mu(\mathbf{s}') \vee \hat{B}_u(\mathbf{s}') < \mu(\mathbf{s}') \quad (E_2 \text{ does not hold})$$

Then, any $c' \in (\mu(\mathbf{s}'), \hat{B}_l(\mathbf{s}'))$ or $c' \in (\hat{B}_u(\mathbf{s}'), \mu(\mathbf{s}'))$,

$$\hat{B}_l(\mathbf{s}') \geq c' \text{ but } \mu(\mathbf{s}') < c'$$

or

$$\mu(\mathbf{s}') \geq c' \text{ but } \hat{B}_u(\mathbf{s}') < c'$$

Contradiction to E_1 . □

A.2 Lemma 1

Lemma 1.

$$E_1 = \left\{ \forall c \in \mathbb{R} : \left(\{\hat{B}_l(\mathbf{s}) \geq c\} \subseteq \{\mu(\mathbf{s}) \geq c\}\right) \wedge \left(\{\mu(\mathbf{s}) \geq c\} \subseteq \{\hat{B}_u(\mathbf{s}) \geq c\}\right) \right\}$$

is equivalent to

$$E'_1 = \left\{ \forall c \in \mathbb{R} : \left(\{\hat{B}_l(\mathbf{s}) > c\} \subseteq \{\mu(\mathbf{s}) > c\}\right) \wedge \left(\{\mu(\mathbf{s}) > c\} \subseteq \{\hat{B}_u(\mathbf{s}) > c\}\right) \right\}$$

Proof. Proof by contradiction for both directions.

Assume E_1 hold and E'_1 does not hold, then $\exists \mathbf{s}' \in \mathcal{S}, \exists c' \in \mathbb{R}, \hat{B}_l(\mathbf{s}') > c' \geq \mu(\mathbf{s}')$ so there exists $\delta > 0$ such that

$$\hat{B}_l(\mathbf{s}') \geq c' + \delta > \mu(\mathbf{s}')$$

This is a contradiction to part of E_1 's statement $\forall c \in \mathbb{R}, \{\hat{B}_l(\mathbf{s}) \geq c\} \subseteq \{\mu(\mathbf{s}) \geq c\}$. Similarly if $\exists \mathbf{s}' \in \mathcal{S}, \exists c' \in \mathbb{R}, \hat{\mu}(\mathbf{s}') > c' \geq \hat{B}_u(\mathbf{s})$ then there exists $\delta > 0$ such that

$$\hat{\mu}(\mathbf{s}') \geq c' + \delta > \hat{B}_u(\mathbf{s})$$

This is a contradiction to the other part of E_1 's statement $\forall c \in \mathbb{R}, \{\mu(\mathbf{s}) \geq c\} \subseteq \{\hat{B}_u(\mathbf{s}) \geq c\}$.

Assume E'_1 hold and E_1 does not hold, then there $\exists \mathbf{s}' \in \mathcal{S}, \exists c' \in \mathbb{R}, \hat{B}_l(\mathbf{s}') \geq c' > \mu(\mathbf{s}')$ so there exists $\delta > 0$ such that

$$\hat{B}_l(\mathbf{s}') > c' - \delta \geq \mu(\mathbf{s}')$$

This is a contradiction to part of E'_1 's statement $\forall c \in \mathbb{R} : \{\hat{B}_l(\mathbf{s}) > c\} \subseteq \{\mu(\mathbf{s}) > c\}$. Similarly if $\exists \mathbf{s}' \in \mathcal{S}, \exists c' \in \mathbb{R}, \mu(\mathbf{s}') \geq c' > \hat{B}_u(\mathbf{s}')$, there exists $\delta > 0$ such that

$$\mu(\mathbf{s}') > c' - \delta \geq \hat{B}_u(\mathbf{s}')$$

This is a contradiction to the other part of E'_1 's statement $\forall c \in \mathbb{R} : \{\mu(\mathbf{s}) > c\} \subseteq \{\hat{B}_u(\mathbf{s}) > c\}$. \square

A.3 Lemma 2

Lemma 2.

$$E_1 = \left\{ \forall c \in \mathbb{R} : \left(\{\hat{B}_l(\mathbf{s}) \geq c\} \subseteq \{\mu(\mathbf{s}) \geq c\} \right) \wedge \left(\{\mu(\mathbf{s}) \geq c\} \subseteq \{\hat{B}_u(\mathbf{s}) \geq c\} \right) \right\}$$

is equivalent to

$$E''_1 = \left\{ \forall a, b \in \mathbb{R}, a < b : \left(\{\hat{B}_l(\mathbf{s}) \geq a \wedge \hat{B}_u(\mathbf{s}) \leq b\} \subseteq \{a \leq \mu(\mathbf{s}) \leq b\} \right) \wedge \left(\{a \leq \mu(\mathbf{s}) \leq b\} \subseteq \{\hat{B}_u(\mathbf{s}) \geq a \wedge \hat{B}_l(\mathbf{s}) \leq b\} \right) \right\}$$

Proof. First, it can be easily seen that E''_1 implies E_1 if we fix $b = +\infty$. Then we show E_1 implies E''_1 by contradiction proof: Assume E_1 hold but E''_1 does not hold, then this means

$$\left\{ \exists a < b \in \mathbb{R} : \left(\{\hat{B}_l(\mathbf{s}) \geq a \wedge \hat{B}_u(\mathbf{s}) \leq b\} \not\subseteq \{a \leq \mu(\mathbf{s}) \leq b\} \right) \right. \quad (\text{A.1})$$

$$\left. \vee \left(\{a \leq \mu(\mathbf{s}) \leq b\} \not\subseteq \{\hat{B}_u(\mathbf{s}) \geq a \wedge \hat{B}_l(\mathbf{s}) \leq b\} \right) \right\} \quad (\text{A.2})$$

A.1 is equivalent to

$$\exists \mathbf{s}' \in \mathcal{S}, \exists a' < b' \in \mathbb{R}, \hat{B}_l(\mathbf{s}') \geq a' \wedge \hat{B}_u(\mathbf{s}') \leq b'$$

but $\mu(\mathbf{s}') > b'$ or $\mu(\mathbf{s}') < a'$. If $\mu(\mathbf{s}') < a'$ then $\hat{B}_l(\mathbf{s}') \geq a' > \mu(\mathbf{s}') \iff \{\hat{B}_l(\mathbf{s}) \geq a\} \not\subseteq \{\mu(\mathbf{s}) \geq a\}$, contradiction to E_1 . If $\mu(\mathbf{s}') > b'$, then $\mu(\mathbf{s}') > b' \geq \hat{B}_u(\mathbf{s}') \iff \{\mu(\mathbf{s}) > b\} \not\subseteq \{\hat{B}_u(\mathbf{s}) > b\}$. By lemma 1, this is a contradiction to E_1 . Similar argument can be made for **A.2**. \square

References

- [1] Keith J Worsley, Alan C Evans, Sean Marrett, and P Neelin. A three-dimensional statistical analysis for cbf activation studies in human brain. *Journal of Cerebral Blood Flow & Metabolism*, 12(6):900–918, 1992.
- [2] Karl J Friston, Keith J Worsley, Richard SJ Frackowiak, John C Mazziotta, and Alan C Evans. Assessing the significance of focal activations using their spatial extent. *Human brain mapping*, 1(3):210–220, 1994.
- [3] John D Storey and Robert Tibshirani. Statistical significance for genomewide studies. *Proceedings of the National Academy of Sciences*, 100(16):9440–9445, 2003.
- [4] Pak C Sham and Shaun M Purcell. Statistical power and significance testing in large-scale genetic studies. *Nature Reviews Genetics*, 15(5):335–346, 2014.

- [5] Henry Scheffe. *The analysis of variance*, volume 72. John Wiley & Sons, 1999.
- [6] Regina Nuzzo. Scientific method: statistical errors. *Nature News*, 506(7487):150, 2014.
- [7] Marko A Hofmann. Searching for effects in big data: Why p-values are not advised and what to use instead. In *2015 Winter Simulation Conference (WSC)*, pages 725–736. IEEE, 2015.
- [8] Monya Baker. Statisticians issue warning over misuse of p values. *Nature News*, 531(7593):151, 2016.
- [9] Alexander Bowring, Fabian JE Telschow, Armin Schwartzman, and Thomas E Nichols. Confidence sets for cohen'sd effect size images. *NeuroImage*, 226:117477, 2021.
- [10] Choong-Wan Woo, Anjali Krishnan, and Tor D Wager. Cluster-extent based thresholding in fmri analyses: pitfalls and recommendations. *Neuroimage*, 91:412–419, 2014.
- [11] Woncheol Jang. Nonparametric density estimation and clustering in astronomical sky surveys. *Computational statistics & data analysis*, 50(3):760–774, 2006.
- [12] Rebecca Willett and Robert Nowak. Level set estimation in medical imaging. In *IEEE/SP 13th Workshop on Statistical Signal Processing, 2005*, pages 1384–1389. IEEE, 2005.
- [13] Alexander Bowring, Fabian Telschow, Armin Schwartzman, and Thomas E Nichols. Spatial confidence sets for raw effect size images. *NeuroImage*, 203:116187, 2019.
- [14] Hanna Jankowski, Xiang Ji, and Larissa Stanberry. A random set approach to confidence regions with applications to the effective dose with combinations of agents. *Statistics in medicine*, 33(24):4266–4278, 2014.
- [15] Joshua P French, Seth McGinnis, and Armin Schwartzman. Assessing narccap climate model effects using spatial confidence regions. *Advances in statistical climatology, meteorology and oceanography*, 3(2):67–92, 2017.
- [16] Asaf Weinstein, William Fithian, and Yoav Benjamini. Selection adjusted confidence intervals with more power to determine the sign. *Journal of the American Statistical Association*, 108(501):165–176, 2013.
- [17] Yuval Benjamini, Jonathan Taylor, and Rafael A Irizarry. Selection-corrected statistical inference for region detection with high-throughput assays. *Journal of the American Statistical Association*, 114(527):1351–1365, 2019.
- [18] Max Sommerfeld, Stephan Sain, and Armin Schwartzman. Confidence regions for spatial excursion sets from repeated random field observations, with an application to climate. *Journal of the American Statistical Association*, 113(523):1327–1340, 2018.
- [19] Enno Mammen and Wolfgang Polonik. Confidence regions for level sets. *Journal of Multivariate Analysis*, 122:202–214, 2013.
- [20] Paula Saavedra-Nieves, Wenceslao González-Manteiga, and Alberto Rodríguez-Casal. A comparative simulation study of data-driven methods for estimating density level sets. *Journal of Statistical Computation and Simulation*, 86(2):236–251, 2016.
- [21] Wanli Qiao and Wolfgang Polonik. Nonparametric confidence regions for level sets: Statistical properties and geometry. *Electronic Journal of Statistics*, 13(1):985–1030, 2019.
- [22] Joshua P French and Stephan R Sain. Spatio-temporal exceedance locations and confidence regions. *The Annals of Applied Statistics*, pages 1421–1449, 2013.
- [23] Joshua P French. Confidence regions for the level curves of spatial data. *Environmetrics*, 25(7):498–512, 2014.
- [24] David Bolin and Finn Lindgren. Excursion and contour uncertainty regions for latent gaussian models. *Journal of the Royal Statistical Society: Series B (Statistical Methodology)*, 77(1):85–106, 2015.
- [25] Kyle Hasenstab, Catherine A Sugar, Donatello Telesca, Kevin McEvoy, Shafali Jeste, and Damla Şentürk. Identifying longitudinal trends within eeg experiments. *Biometrics*, 71(4):1090–1100, 2015.
- [26] Kyle Hasenstab, Catherine Sugar, Donatello Telesca, Shafali Jeste, and Damla Şentürk. Robust functional clustering of erp data with application to a study of implicit learning in autism. *Biostatistics*, 17(3):484–498, 2016.
- [27] Jelle J Goeman and Aldo Solari. Multiple testing for exploratory research. *Statistical Science*, 26(4):584–597, 2011.
- [28] Jelle J Goeman, Jesse Hemerik, and Aldo Solari. Only closed testing procedures are admissible for controlling false discovery proportions. *The Annals of Statistics*, 49(2):1218–1238, 2021.
- [29] David Degras. Simultaneous confidence bands for the mean of functional data. *Wiley Interdisciplinary Reviews: Computational Statistics*, 9(3):e1397, 2017.
- [30] David A Degras. Simultaneous confidence bands for nonparametric regression with functional data. *Statistica Sinica*, pages 1735–1765, 2011.

- [31] Guanqun Cao. Simultaneous confidence bands for derivatives of dependent functional data. *Electronic Journal of Statistics*, 8(2):2639–2663, 2014.
- [32] Yueying Wang, Guannan Wang, Li Wang, and R Todd Ogden. Simultaneous confidence corridors for mean functions in functional data analysis of imaging data. *Biometrics*, 76(2):427–437, 2020.
- [33] Chung Chang, Xuejing Lin, and R Todd Ogden. Simultaneous confidence bands for functional regression models. *Journal of Statistical Planning and Inference*, 188:67–81, 2017.
- [34] Fabian JE Telschow and Armin Schwartzman. Simultaneous confidence bands for functional data using the gaussian kinematic formula. *Journal of Statistical Planning and Inference*, 216:70–94, 2022.
- [35] Fang Yao, Hans-Georg Müller, and Jane-Ling Wang. Functional data analysis for sparse longitudinal data. *Journal of the American statistical association*, 100(470):577–590, 2005.
- [36] Shujie Ma, Lijian Yang, and Raymond J Carroll. A simultaneous confidence band for sparse longitudinal regression. *Statistica Sinica*, 22:95, 2012.
- [37] Yuhyun Park, Sean R Downing, Dohyun Kim, William C Hahn, Cheng Li, Philip W Kantoff, and LJ Wei. Simultaneous and exact interval estimates for the contrast of two groups based on an extremely high dimensional variable: application to mass spec data. *Bioinformatics*, 23(12):1451–1458, 2007.
- [38] JT Gene Hwang and Zhigen Zhao. Empirical bayes confidence intervals for selected parameters in high-dimensional data. *Journal of the American Statistical Association*, 108(502):607–618, 2013.
- [39] Jing Qiu and JT Gene Hwang. Sharp simultaneous confidence intervals for the means of selected populations with application to microarray data analysis. *Biometrics*, 63(3):767–776, 2007.
- [40] Vijayan N Nair. Confidence bands for survival functions with censored data: a comparative study. *Technometrics*, 26(3):265–275, 1984.
- [41] MI Parzen, LJ Wei, and Z Ying. Simultaneous confidence intervals for the difference of two survival functions. *Scandinavian Journal of Statistics*, 24(3):309–314, 1997.
- [42] Ian W McKeague and Yichuan Zhao. Simultaneous confidence bands for ratios of survival functions via empirical likelihood. *Statistics & Probability Letters*, 60(4):405–415, 2002.
- [43] Wei Liu, Shan Lin, and Walter W Piegorsch. Construction of exact simultaneous confidence bands for a simple linear regression model. *International Statistical Review*, 76(1):39–57, 2008.
- [44] Jiayang Sun and Clive R Loader. Simultaneous confidence bands for linear regression and smoothing. *The Annals of Statistics*, pages 1328–1345, 1994.
- [45] Walter W Piegorsch and George Casella. Confidence bands for logistic regression with restricted predictor variables. *Biometrics*, pages 739–750, 1988.
- [46] David A Freedman. Bootstrapping regression models. *The Annals of Statistics*, 9(6):1218–1228, 1981.
- [47] Cun-Hui Zhang and Stephanie S Zhang. Confidence intervals for low dimensional parameters in high dimensional linear models. *Journal of the Royal Statistical Society: Series B (Statistical Methodology)*, 76(1):217–242, 2014.
- [48] Brandreth Symonds. The blood pressure of healthy men and women. *Journal of the American Medical Association*, 80(4):232–236, 1923.
- [49] LOea Mearns, Seth McGinnis, Raymond Arritt, Sebastien Biner, Phillip Duffy, William Gutowski, Isaac Held, Richard Jones, Ruby Leung, Ana Nunes, et al. The north american regional climate change assessment program dataset. *National Center for Atmospheric Research Earth System Grid data portal, Boulder, CO*, 10:D6RN35ST, 2007.
- [50] Linda O Mearns, William Gutowski, Richard Jones, Ruby Leung, Seth McGinnis, Ana Nunes, and Yun Qian. A regional climate change assessment program for north america. *Eos, Transactions American Geophysical Union*, 90(36):311–311, 2009.
- [51] Joeri Rogelj, Bill Hare, Julia Nabel, Kirsten Macey, Michiel Schaeffer, Kathleen Markmann, and Malte Meinshausen. Halfway to copenhagen, no way to 2 c. *Nature Climate Change*, 1(907):81–83, 2009.
- [52] Kevin Anderson and Alice Bows. Beyond ‘dangerous’ climate change: emission scenarios for a new world. *Philosophical Transactions of the Royal Society A: Mathematical, Physical and Engineering Sciences*, 369(1934):20–44, 2011.
- [53] Vincenzo Castiglione, Martina Chiriacò, Michele Emdin, Stefano Taddei, and Giuseppe Vergaro. Statin therapy in covid-19 infection. *European Heart Journal-Cardiovascular Pharmacotherapy*, 6(4):258–259, 2020.

[54] Lori B Daniels, Amy M Sitapati, Jing Zhang, Jingjing Zou, Quan M Bui, Junting Ren, Christopher A Longhurst, Michael H Criqui, and Karen Messer. Relation of statin use prior to admission to severity and recovery among covid-19 inpatients. *The American journal of cardiology*, 136:149–155, 2020.